Volume 45 | Number 17 | 7 May 2016 | Pages 7181–7522

# Dalton Transactions

An international journal of inorganic chemistry

www.rsc.org/dalton

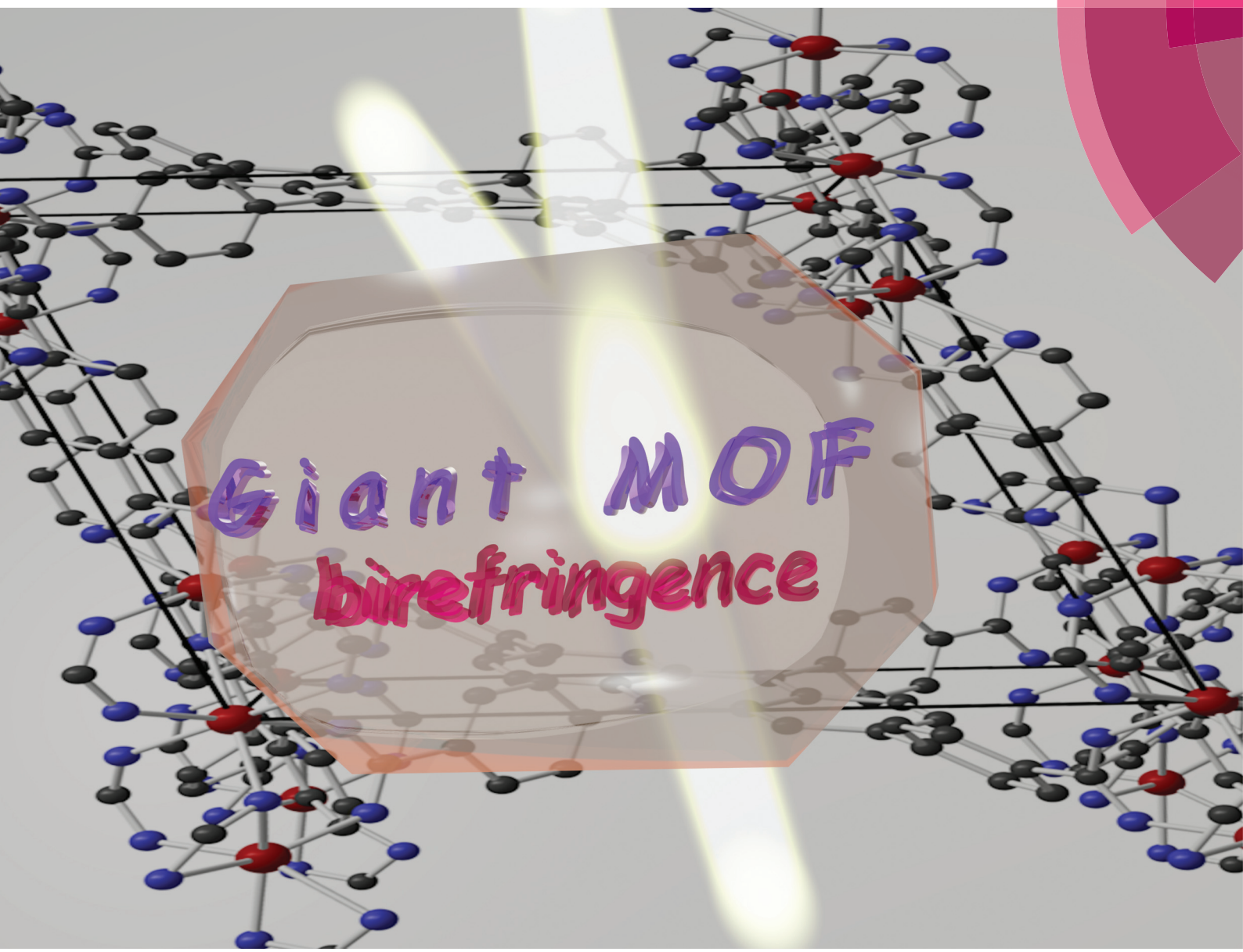


ISSN 1477-9226

ROYAL SOCIETY OF CHEMISTRY

PAPER

A. V. Vinogradov, E. Hey-Hawkins *et al.*

Unique anisotropic optical properties of a highly stable metal–organic framework based on trinuclear iron(III) secondary building units linked by tetracarboxylic linkers with an anthracene core

175 YEARS

Dalton Transactions

PAPER

View Article Online
View Journal | View Issue

Open Access Article. Published on 12 February 2016. Downloaded on 2/14/2026 7:53:12 AM.
This article is licensed under a Creative Commons Attribution-NonCommercial 3.0 Unported Licence.

Cite this: *Dalton Trans.*, 2016, **45**, 7244

# Unique anisotropic optical properties of a highly stable metal–organic framework based on trinuclear iron(III) secondary building units linked by tetracarboxylic linkers with an anthracene core†

A. V. Vinogradov,*[a] V. A. Milichko,[a] H. Zaake-Hertling,[b] A. Aleksovska,[b] S. Gruschinski,[b] S. Schmorl,[b] B. Kersting,[b] E. M. Zolnhofer,[c] J. Sutter,[c] K. Meyer,[c] P. Lönnecke[b] and E. Hey-Hawkins*[b]

Received 27th January 2016,
Accepted 12th February 2016

DOI: 10.1039/c6dt00390g

www.rsc.org/dalton

A highly stable metal–organic framework, $[\{Fe_3(ACTBA)_2\}X{\cdot}6DEF]_n$ (**1**; X = monoanion), based on trinuclear iron(III) secondary building units connected by tetracarboxylates with an anthracene core, 2,6,9,10-tetrakis-(*p*-carboxylatophenyl)anthracene (ACTBA), is reported. Depending on the direction of light polarisation, crystals of **1** exhibit anisotropic optical properties with birefringence $\Delta n = 0.3$ ($\lambda = 590$ nm).

## Introduction

Metal–organic frameworks (MOFs) are an attractive class of porous solids with potential applications in gas storage and separation, energy conversion and catalysis.[1–5] All of these versatile physical and chemical properties or niche applications have been shown to be heavily reliant on their unique structures. On the other hand, Fe-based MOFs have attracted wide scientific attention owing to their low toxicity and magnetic properties, medical and biological functions (drug release, imaging) and application in lithium-ion batteries and hydrocarbon separations.[6–8] However, most recent research has concentrated on the exploration of Cu- and Zn-based MOFs,[1a] while studies on Fe-based MOFs are relatively scarce.[5] The main reason is the difficulty in controlling methodology and experimental conditions, as iron salts exhibit a strong tendency to undergo hydrolysis resulting in stable hydrated iron oxide and precipitation instead of crystallisation.[9]

The research presented here is focused on a tetratopic anthracene-based ligand, namely, 2,6,9,10-tetrakis(*p*-carboxylatophenyl)anthracene (referred to as anthracene tetrabenzoate (ACTBA), Fig. 1), as conjugated or fused aromatic compounds may exhibit interesting optical features, acting as charge donors or acceptors. Furthermore, with iron ions, such compounds are capable of exhibiting unique optical properties due to strong spatial anisotropy on the nanoscale, as was discovered for the first time in this class of materials described here. This feature opens up broad prospects for the use of MOF single crystals in managing photoexcitation under the influence of light.[10]

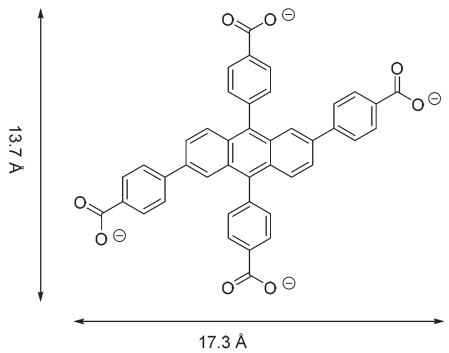


**Fig. 1** The tetracarboxylate linker, ACTBA.

## Results and discussion

Single crystals of $[\{Fe_3(ACTBA)_2\}X{\cdot}6DEF]_n$ (**1**; X = monoanion) were obtained by solvothermal synthesis from $FeCl_3{\cdot}6H_2O$ and the corresponding acid of the linker, $H_4$-ACTBA, in diethylformamide (DEF). The colour of the crystals ranges from dark yellow to brown, depending on their thickness and the angle of incidence of a light beam. Compound **1** crystallises in the triclinic

[a]*ITMO University, St. Petersburg, 197101, Russian Federation. E-mail: vinogradoffs@gmail.com*
[b]*Leipzig University, Faculty of Chemistry and Mineralogy, Institute of Inorganic Chemistry, D-04103 Leipzig, Germany. E-mail: hey@uni-leipzig.de*
[c]*Friedrich-Alexander University Erlangen – Nürnberg (FAU), Department of Chemistry & Pharmacy, Inorganic Chemistry, D-91058 Erlangen, Germany*

†Electronic supplementary information (ESI) available: **1**: X-ray powder diffraction, determination of the surface area, different views of the 3D structure, magnetic susceptibility, Mößbauer spectroscopy, EPR measurements, DTA-TG, optical properties. CCDC 1062660. For crystallographic data in CIF or other electronic format see DOI: 10.1039/c6dt00390g


This journal is © The Royal Society of Chemistry 2016

Open Access Article. Published on 12 February 2016. Downloaded on 2/14/2026 7:53:12 AM.
This article is licensed under a Creative Commons Attribution-NonCommercial 3.0 Unported Licence.

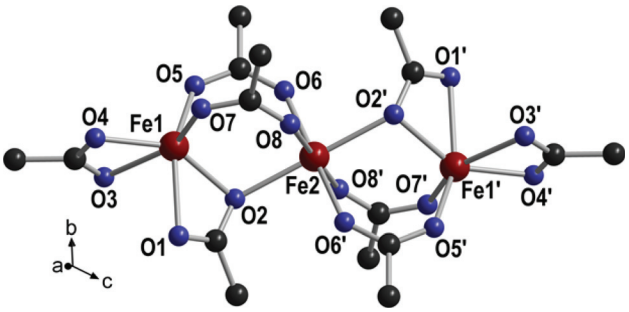


Fig. 2 The SBU $Fe_3(RCO_2)_8$.

space group $P\bar{1}$ (see ESI, Table S1†) forming a porous network consisting of $Fe_3(RCO_2)_8$ as a secondary building unit (Fig. 2).

The central iron atom (Fe2) is located on a crystallographic inversion centre and exhibits perfect octahedral coordination, whereas the coordination environment of Fe1/Fe1′ is best described as distorted tetrahedral if the two chelating carboxylato groups are regarded as occupying one coordination site. The eight carboxylato groups belong to eight separate ACTBA linkers and exhibit different bonding modes: four are $\mu_2,\kappa^1{:}\kappa^1$ (between Fe1 or Fe1′ and Fe2), two are $\mu_2,\kappa^2{:}\kappa^1$ ($\kappa^2$ at Fe1 or Fe1′ and $\kappa^1$ at Fe2), and two are $\kappa^2$ (at Fe1 and Fe1′). With respect to the planar anthracene core, the four phenylene substituents exhibit different angles between the ring planes, which range from 40.0 to 73.8° (see ESI, Fig. S11 and Table S2†). The resulting structure (Fig. 3) is highly porous and exhibits channels along the *a*, *b* and *c* axes (Fig. 4) as well

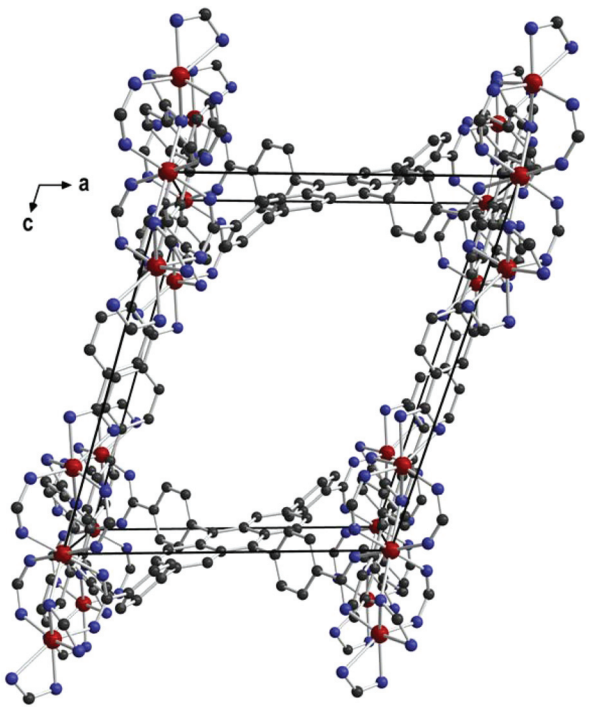


Fig. 3 View along the *b* axis in **1** showing one pore (B) and the connectivity of the linkers.

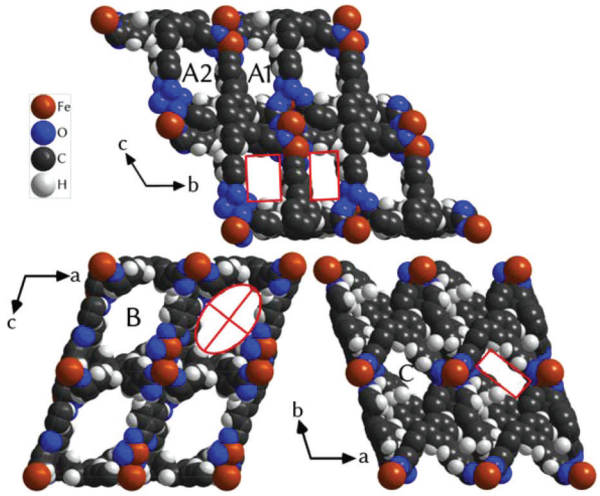


Fig. 4 Views along the *a*, *b* and *c* axes in **1** showing the different pores.

as in other directions (see ESI, Fig. S4†). Viewed along the *a* axis, two different pores are observed, labelled A1 (*ca.* 6.4 × 4.0 Å) and A2 (*ca.* 5.8 × 4.9 Å); the largest pores are observed along the *b* axis (B, *ca.* 12.0 × 7.5 Å), and the smallest along the *c* axis (C, *ca.* 7.2 × 2.6 Å) (Fig. 4; the pore dimensions were obtained from space-filling models based on van der Waals radii).

All attempts to locate solvent molecules inside the pores failed due to their high disorder. Therefore, these molecules were removed with the SQUEEZE routine implemented in PLATON; the electron count suggests the presence of six poorly defined DEF molecules in the unit cell. Furthermore, as magnetic measurements and Mößbauer spectroscopy indicate the presence of three $Fe^{III}$ cations, an anion X [possibly hydroxide or formate (from decomposition of DEF) besides 10% chloride] must be present for charge neutrality.

TG-DTA analysis was carried out in the range of 30–700 °C and showed **1** to be stable up to 350 °C (see ESI, Fig. S9†). The thermal stability is comparable to that of MIL-53,[11] whereby the high stability may be due to the high valence of the metal ions and the connectivity of the SBU rods.[12,13] Also, the recently reported MOFs ROD-6 and ROD-7, based on Mn or In and 1,3,6,8-tetrakis(*p*-carboxylatophenyl)pyrene as linker, exhibit similar stability.[12]

The permanent porosity of an activated sample was confirmed by the $N_2$ sorption isotherm at 77 K (see ESI, Fig. S2†). The microporosity was assessed by using the Langmuir and BET theories for surface area analysis and the Dubinin–Astakhov (DA) method for pore size distribution (see ESI, Fig. S3†). The BET and Langmuir surface areas are 554 and 715 $m^2\ g^{-1}$, respectively, which were calculated from the nitrogen physisorption data in the relative pressure range $p/p_0$ = 0.06–0.30. The total pore volume of **1** based on this method is 0.164 $cm^3\ g^{-1}$ associated with an average pore radius of 5.2 Å (DA). The data obtained are in accord with the pore volumes calculated by using the program package Platon.[14] However, in the structure determination, the SQUEEZE analysis revealed a total volume

Open Access Article. Published on 12 February 2016. Downloaded on 2/14/2026 7:53:12 AM.
This article is licensed under a Creative Commons Attribution-NonCommercial 3.0 Unported Licence.

of 1.978 $nm^3$ for the solvent-accessible area of the unit cell. This corresponds to a pore volume of 0.56 $cm^3\ g^{-1}$, which is 3.5 times higher than the value that was deduced from the Barrett–Joyner–Halenda (BJH) analysis.

In order to understand the electronic structure of the trinuclear SBU in **1**, microcrystalline samples were studied by VT-SQUID, VT-CW X-band EPR and zero-field $^{57}$Fe Mößbauer spectroscopy at 77 K (see ESI, Fig. S6†). The SQUID magnetisation measurement (see ESI, Fig. S5†), recorded in the temperature range 2–300 K, revealed a reproducible, strongly temperature-dependent magnetic moment over the entire temperature range. The magnetic moment at 2 K was determined to be 3.9 $\mu_B$, and thus indicates an $S_{tot}$ = 3/2 ground state for the SBU. With increasing temperature, the magnetic moment increases steadily to give a value of approximately 11 $\mu_B$ at room temperature. The zero-field Mößbauer spectrum of **1**, recorded at 77 K (see ESI, Fig. S6†), shows one symmetric quadrupole doublet with an isomer shift $\delta$ of 0.52 mm $s^{-1}$ and a quadrupole splitting $\Delta E_Q$ of 0.70 mm $s^{-1}$. These Mößbauer parameters are characteristic for high-spin iron(III) ions ($Fe^{3+}$, $d^5$, $S$ = 5/2) in an O-donor ligand environment. However, a single Mößbauer feature appears to be inconclusive and not in agreement with the trinuclear SBU, as the Fe centres in **1** have significantly different ligand environments. The outer Fe ions (Fe1, Fe1′) are best described as being situated in a tetrahedral coordination sphere, while the central ion (Fe2) is clearly octahedrally coordinated. Accordingly, one would expect two Mößbauer signals with an intensity ratio of 2 : 1. In principle, if both Fe sites were high-spin $S$ = 5/2, they could have similar Mößbauer parameters. With that said, the observation of a relatively sharp ($\Gamma_{FWHM}$ = 0.57 mm $s^{-1}$) and symmetric doublet still would not be anticipated. In addition, the formulation of three magnetically coupled high-spin Fe ions cannot result in an electronic ground state $S_{tot}$ of 3/2, as suggested by SQUID magnetisation. An EPR spectroscopic study remains equally inconclusive. CW X-band EPR spectra of two batches, recorded at 8 and 6 K (see ESI, Fig. S7 and S8†), show very similar features with identical $g$ values. A signal at $g$ = 8.47 and 4.13 is indicative for an $S$ = 5/2 ion, for which the expected high-field third resonance is broadened into the baseline or hidden underneath the second, rhombic signal centred at $g$ = 1.81, 2.00 and 2.18. Although these signals are remarkably reproducible, their intensities are not and, furthermore, they are not in the expected integer ratio of 2 : 1 to each other. Accordingly, a temperature-dependent EPR study (6–290 K, see ESI, Fig. S8†) was carried out. Clearly, with increasing temperature, the low-field feature at $g \approx 8.5$ and 4 loses signal intensity, while the resonance at $g \approx 2$ shifts to slightly lower fields, resulting in a single, broad resonance centred at $g$ = 2.64, 1.97 and 1.90. The coalescence temperature of about 80–100 K could explain the single quadrupole doublet observed in the $^{57}$Fe Mößbauer spectrum (recorded at 77 K). In conclusion, the magnetochemical study (see ESI†) suggests that the electronic structure of **1** cannot be described as an electronically isolated, trinuclear, molecular Fe moiety. Instead, the spectroscopic data suggest that the SBUs engage in intermolecular interactions, most likely in addition to intramolecular magnetic superexchange. Accordingly, a simple interpretation of the electronic structure of supramolecular **1** on a molecular level (the SBU) is severely hampered by spin–spin interactions, as is most obviously seen in the VT EPR study. This leads to complicated magnetic phenomena, detailed interpretation of which is beyond the scope of this work.

From a physical point of view, a central feature of the crystal structure of **1** are the ordered $Fe^{III}$ cations forming atomically thin metal-ion chains and defined nanoscale channels. Objects with such structural features have strongly anisotropic physical properties,[15] for instance, optical or conductive properties. At best, they may have unique metamaterial properties[16a] due to the combination of metallic (Fe chains) and dielectric elements (channels) in a single crystal. The latter is enhanced by the fact that all single elements are nanoscale and can be considered as a quantum system. In turn, this is essential for quantum metamaterials.[16b] Basically, classical optical studies on MOF conglomerates and arrays strongly dominate over specific studies on single crystals of MOFs, which are mostly dedicated to luminescence.[17] Therefore, studies of the anisotropy of the optical properties of **1** were carried out. The transmission/reflection spectra (experimental setup described in ESI, Fig. S10†) obtained for a single crystal at two orthogonal polarisations ($E_1$ and $E_2$) were normalised by the spectra acquired under the same conditions from the slide in DEF (Fig. 5). Here, the transmission spectra $T$ were recalculated to optical densities OD (OD = $-\lg T$), which in turn can be considered as characteristic of absorption $A$ of radiation in a crystal of length $L$ ($A$ = 2.3 OD/$L$).

For single crystals of **1** it can be concluded that the different amplitudes and shapes of the reflectance/absorption spectra for light with orthogonal polarisations ($E_1$ and $E_2$) indicate a strong anisotropy of the optical properties (Fig. 5): (i) different band gap for light with orthogonal polarisation (2.7 eV *versus* 2.4 eV), and (ii) anisotropy of the refractive index $n$. The refractive indices of **1** in the case of normal incidence of light on a homogeneous dielectric film (*i.e.*, single crystal of **1**)[18] can be obtained from the following expression:

$$R = [(n_1 n_2 - n^2)/(n_1 n_2 + n^2)]^2$$

where $R$ is the reflectance and $n_1$, $n_2$ are the refractive indices of the slide (1.51)[19] and DEF (1.433)[20] in the visible range. Obtained spectra (Fig. 5) indicate that a single crystal of **1** has a giant difference of $n$ within the whole visible range. In particular, **1** has refractive indices of 1.84 and 2.14 for $E_1$ and $E_2$ polarisation at a wavelength of 590 nm ($\Delta n$ = 0.3), the sodium D line, which is in the same range as well-known and widely used commercial anisotropic crystals (calcite, rutile, sodium nitrate, calomel)[21] with extremely large birefringence at the same wavelength ($0.17 < \Delta n < 0.68$). For the whole visible range, the value of $\Delta n$ varies from 0.19 to 0.34. However, the geometry of the optical experiment is not optimal due to the fact that we do not know the orientation of the $Fe^{III}$ cations and optical axes with respect to the sides of the crystal of **1** (insert in Fig. 5). Therefore, it can be argued that $\Delta n$ can reach

 This journal is © The Royal Society of Chemistry 2016

Open Access Article. Published on 12 February 2016. Downloaded on 2/14/2026 7:53:12 AM.
This article is licensed under a Creative Commons Attribution-NonCommercial 3.0 Unported Licence.

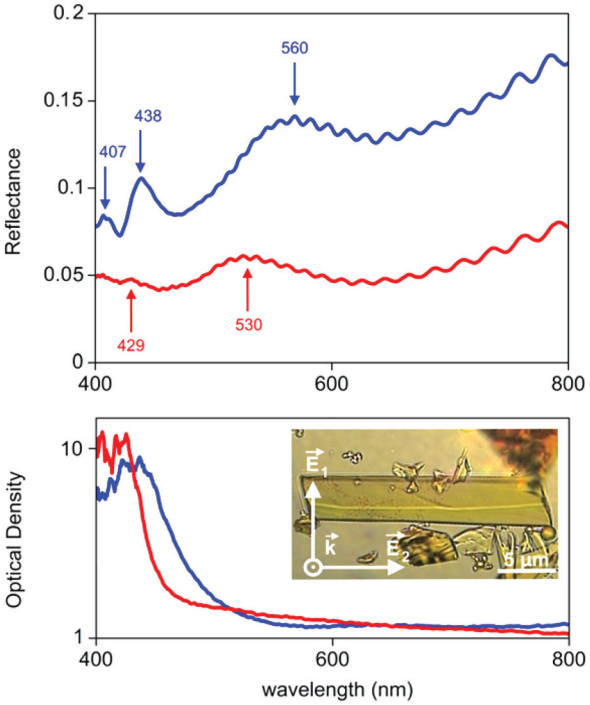


**Fig. 5** Reflectance spectra and optical density of a single crystal of **1** irradiated perpendicular to its surface. Red and blue curves correspond to reflection/absorption of electromagnetic waves with electric vectors E which are perpendicular ($E_1$) or parallel ($E_2$) to the longest side of the crystal, as shown in the inset. The oscillations in the reflectance spectra indicate interference in thin films, and the calculated optical thickness of the crystal shown is 10 μm. The slope of the optical density curves supports different band gaps of **1** depending on light polarisation (2.7 eV for $E_1$ and 2.4 eV for $E_2$).

much larger values than 0.3 in case of optimal propagation of electromagnetic waves with orthogonal polarisations.

Also a higher value of birefringence can be achieved in nanostructured semiconductors[22] or liquid crystals.[23] However, the former is valid for the IR range due to small band gaps, and the latter has a restriction on ultrafast operation.

Polarised transmittance and reflectance spectroscopy was carried out for 13 single crystals of **1** with lateral dimension from 2 to 20 μm showing consistent anisotropic optical properties. The observed optical anisotropy directly results from the crystal structure of **1**. Due to the charge-transfer properties of the anthracene derivative (ACTBA)[24] and metal-ion chains ordered in different spatial directions, crystals with a structural period of less than 1 nm have anisotropic permittivity and metallic features in the visible spectral range. As a result, the interaction between polarised optical radiation and a single crystal of **1** results in the above-mentioned properties.

## Conclusions

In conclusion, the novel highly porous MOF reported here based on a tetracarboxylic linker with an anthracene core (ACTBA) and an $Fe_3(RCO_2)_8$ SBU reveals giant optical anisotropy arising from metal-ion chains ordered in different spatial directions allowing the single crystals to change their reflectance/absorption depending on the direction of the polarisation vector. We expect that this study, performed for the first time on individual microcrystals, will motivate investigations of other anisotropic properties of single crystals of MOFs and will thus open up unprecedented new applications.

## Experimental

### General methods

**Reaction vessels.** Stainless steel vessels (autoclaves, made from (X5CrNiMo17-12-2) AISI 316 aka V4A) with PTFE liners (about 20 ml) were used for the reactions. Solvothermal/temperature-controlled reactions took place in Memmert ovens models UFE400 and UNE600 controlled *via* computer software over RS-232. Unless otherwise noted, chemicals and solvents were used as purchased. Solvents were dried with an MBRAUN SPS-800. DEF was dried with $Na_2SO_4$, then stirred at room temperature for 2 h with $CaH_2$ followed by filtration and distillation under reduced pressure. Silica used was Merck VWR Geduran Si60 (40–60 μm). Anthracene was used as purchased. Boronic acid was prepared from destilled *p*-bromotoluene *via* boronation and, in case of 4-carboxyphenylboronic acid, followed by oxidation and esterification. 4-Methoxycarbonylphenylboronic acid is also commercially available. 4-Methoxycarbonylphenylboronic acid was always a mixture of free acid and boroxine (trimeric anhydride), but both compounds can be employed in the reaction. 2,6,9,10-Tetrabromoanthracene was prepared according to ref. 25. NMR spectra were recorded with a Bruker AVANCE DRX 400 spectrometer; chemical shifts are given in parts per million (ppm) at 400.13 ($^1$H). Internal standard was TMS (tetramethylsilane). Infrared spectra were recorded on a Perkin-Elmer FT-IR Spectrum 2000 spectrometer in KBr. Elemental analysis was conducted with a VARIO EL (Heraeus). ESI-MS was performed with a Bruker Esquire 3000 plus, for EI-MS a Finnigan MAT 8230 (70 eV) was used. Melting points were determined with a Gallenkamp MPD350.BM2.5 device.

**Synthesis of $H_4$-ACTBA.** $Me_4$-ACTBA was prepared from 2,6,9,10-tetrabromoanthracene and 1-COOMe-4-B(OH)$_2$-$C_6H_4$ *via* Suzuki–Miyaura coupling (general protocol in ref. 26). Oxygen-free dioxane and deionised and degassed water (ratio 3 : 1) were added *via* cannula to a mixture of 2,6,9,10-tetrabromoanthracene (1 eq.), boronic acid (in total 5.8 to 6.6 eq. of 1-COOMe-4-B(OH)$_2$-$C_6H_4$, starting with 3 eq. and adding additional portions of 1.2 eq. after 3, 6 and 9 days), base (7.5 eq. $Na_2CO_3$) and catalyst ([Pd(PPh$_3$)$_4$], 1.5 mol%) under nitrogen. The mixture was refluxed for 10–12 days. Additional boronic acid was added after every third day. Solvent was removed on a rotary evaporator. Purification can be achieved by column chromatography using *n*-hexane/ethyl acetate (8 : 1) with a rising gradient of ethyl acetate as eluent on silica.

Open Access Article. Published on 12 February 2016. Downloaded on 2/14/2026 7:53:12 AM.
This article is licensed under a Creative Commons Attribution-NonCommercial 3.0 Unported Licence.

$Me_4$-ACTBA is soluble in warm and polar organic solvents as well as in aromatic solvents. M.p.: decomp. without melting. Analytical data for $Me_4$-ACTBA: $^1$H-NMR ($CDCl_3$, $\delta$ in ppm): 8.34 (d, 8.2 Hz, 4 H, presumably pos. 3′/5′ or 3″/5″), 8.07 (d, 8.2 Hz, 4 H, presumably pos. 3′/5′ or 3″/5″), 7.87 (d, *ca.* 1.3 Hz, 2 H, 1,5-pos.), 7.74 (d, *ca.* 9.1 Hz, 2 H, 4,8-pos.), 7.67–7.64 (m/overlap, 6 H, presumably pos. 3,7 and 2′/6′ or 2″/6″), 7.59 (d, 8.2 Hz, 4 H, presumably pos. 2′/6′ or 2″/6″), 4.04 (s, 6 H, Me), 3.92 (s, 6 H, Me); it is assumed that positions 1,3 and 5,7 couple *via* $^4J_{H-H}$; coupling constants in this area are hard to obtain with certainty. Related compounds with a similar substitution pattern (*e.g.* 2,6-dibromo-9,10-anthraquinone) show a distinct $^4J_{H-H}$ for these positions. MS (ESI+, DCM/MeOH; [*m*/*z*]): 715.5 $[M + H]^+$, 737.2 $[M + Na]^+$. IR ($\tilde{\nu}$ in $cm^{-1}$): 3437 (br s, $H_2O$), 3080–2970 (several w), 2953 (w), 2847 (w), 2380–2320 (several w), 2078 (br w), 1724 (vs), 1680 (m/w–w), 1653 (m/w–w), 1608 (s), 1570–1500 (several w), 1456 (m/w–w), 1436 (m), 1404 (w), 1378 (w), 1279 (br, vs), 1192 (m/w), 1180 (m/w), 1113 ((br) s), 1019 (m/w), 951 (m/w–w), 916 (w), 889 (w), 858 (m/w–w), 819 (m/w–w), 771 (m), 737 (w), 709 (m/w), 640–580 (several w), 530–418 (several w). Found C, 74.99%; H, 4.68%; calcd for $C_{46}H_{34}O_8$ × 1/3 DCM (DCM from workup): C, 74.89%; H, 4.70%.

$H_4$-ACTBA was obtained by saponification by adding aqueous NaOH and refluxing overnight. Dioxane was removed on a rotary evaporator. If necessary, more water was added. The warm mixture was filtrated and the solid washed with water. The basic filtrate (clear yellow solution) was poured slowly into ice/water/HCl (aq) under stirring. The product precipitated as a bright yellow powder. The product was isolated by filtration, washed with hot water and dried in vacuum at 140 °C for several hours yielding a yellow powder. Typical yields: 80–86% (4.9 to 12.3 g). The product is not soluble in aliphatic solvents, slightly soluble in alcohols at room temperature (esp. $^i$PrOH), better at elevated temperature. M.p.: decomp. without melting. Analytical data for $H_4$-ACTBA: $^1$H-NMR (DMSO-d6, *d* in ppm): 7.67 (d, *ca*. 2 H, *ca.* 1.5 Hz), 7.70–7.73 (m(?), *ca*. 6 H), 7.74 (s, *ca*. 2 H), 7.84 (s, 2 H, probably 1,5-position, possibly d, 1.5 Hz), 7.87 (probably dd, 2 H, 9 Hz and small d of *ca.* 1.5 Hz, likely 3,7-position because of possible $^4J_{H-H}$ with 1,5-position), 8.02 (d, 4 H, *ca.* 8 Hz), 8.28 (d, 4 H, *ca.* 8 Hz); COOH not observed. The overlapping signals from 7.67 to 7.74 ppm integrate to *ca.* 10 H. MS (ESI–, MeOH; [*m*/*z*]): 328.0 $[M - 2H]^{2-}$, 657.1 $[M - H]^-$, 679.0 $[M - 2H + Na]^-$. IR ($\tilde{\nu}$ in $cm^{-1}$): 3456 (br s, $H_2O$), 2964 (m), 1691 (br s), 1609 (s), 1568 (w), 1409 (br m), 1262 (m/s), 1178 (w/m), 1103 (m), 1019 (w/m), 951 (w), 860 (w), 801 (m), 708 (w). Found C, 75.17%; H, 4.02%; calcd for $C_{42}H_{26}O_8 \times 0.5H_2O$: C, 75.55%; H, 4.08%.

**Synthesis of 1.** About 0.08 mmol of the anthracene-based ligand ($H_4$-ACTBA) were dissolved in 3 ml DEF (DEF was used rather than DMF as the latter hydrolyses much more rapidly with formation of formate and dimethylamine) and added to the Teflon liner with *ca.* 0.6 mmol $FeCl_3 \cdot 6H_2O$. Temperature programme: 5 h rising to 180 °C, keeping at 180 °C for 28 h and decreasing over 48 h to rt. After the reaction, the crystalline material was isolated, washed twice with MeOH and dried at room temperature. The colour of the crystals ranges from a dark yellow to brown (depending on thickness and light). IR ($\tilde{\nu}$ in $cm^{-1}$): 3438 (br, $H_2O$), 2965 (m), 1691 (m), 1658 (m), 1652 (m), 1607 (br s), 1558–1502 (br, several absorptions, m), 1404 (br s), 1262 (s), 1178 (m), 1098 (br s), 1019 (s), 950 (m/w), 862 (m/w), 803 (s), 709 (m/w), 626 (w), *ca.* 502 (several absorptions, w).

### Crystal structure determination

The X-ray data were collected on a Gemini-S CCD diffractometer (Agilent Technologies) using Mo-$K_\alpha$ radiation ($\lambda$ = 0.71073 Å), $\omega$-scan rotation. Data reduction was performed with CrysAlis Pro,[27] including the program SCALE 3 ABSPACK[28] for empirical absorption correction. Structure solution with SHELXS-2013 (direct method). Anisotropic refinement of all non-hydrogen atoms with SHELXL-2014.[29] Hydrogen atoms are calculated on idealised positions. Solvent molecules were removed with the SQUEEZE routine implemented in PLATON.[14] Figures were drawn with Diamond v 3.2i. Structural data of **1**: $C_{114}H_{110}ClFe_3N_6O_{22}$ ({$Fe_3$(ACTBA)$_2$}X·6DEF), $M$ = 2119.07, triclinic, space group $P\bar{1}$, $a$ = 13.3774(7) Å, $b$ = 17.0481(7) Å, $c$ = 17.4322(7) Å, $\alpha$ = 118.491(4)°, $\beta$ = 99.961(4)°, $\gamma$ = 100.101(4)°, $V$ = 3285.1(3) $Å^3$, $Z$ = 1, $\rho_{calcd}$ = 1.071 Mg $m^{-3}$, $\mu$ = 0.407 $mm^{-1}$, $\Theta_{max.}$ = 26.37°, $R_{(all\ data)}$ = 0.0817, $R_{w(all\ data)}$ = 0.1772, $T$ = 130(2) K, 13 416 independent reflections, 466 parameters, no restraints, maximal residual electron density 0.618 e $Å^{-3}$. CCDC 1062660 (**1**) contains the supplementary crystallographic data for this paper.

## Acknowledgements

We gratefully acknowledge financial support from Leipzig University, the DAAD (postdoctoral grant for A. V. V., doctoral grant to A. A. (GSSP)) and the ERASMUS+ mobility program, the Russian Government, Ministry of Education (research was made possible due to funds provided aiming at maximising ITMO University's competitive advantage among world's leading educational centres) and Russian Foundation for Basic Research (grant no. 16-37-60073 mol_a_dk).

## References

1 (*a*) W. Xuan, C. Zhu, Y. Liu and Y. Cui, *Chem. Soc. Rev.*, 2012, **41**, 1677–1695; (*b*) A. Vinogradov, H. Zaake-Hertling, E. Hey-Hawkins, A. V. Agafonov, G. A. Seisenbaeva, V. G. Kessler and V. V. Vinogradov, *Chem. Commun.*, 2014, **50**, 10210–10213.

2 C. Volkringer, D. Popov, T. Loiseau, N. Guillou, G. Férey, M. Haouas, F. Taulelle, C. Mellot-Draznieks, M. Burghammer and C. Riekel, *Nat. Mater.*, 2007, **6**, 760–764.

3 S. Kitagawa, Y. Kubota, R. V. Belosludov, T. C. Kobayashi, H. Sakamoto, T. Chiba, M. Takata, Y. Kawazoe and Y. Mita, *Nature*, 2005, **436**, 238–241.

 This journal is © The Royal Society of Chemistry 2016

Open Access Article. Published on 12 February 2016. Downloaded on 2/14/2026 7:53:12 AM.
This article is licensed under a Creative Commons Attribution-NonCommercial 3.0 Unported Licence.

4 M. Sindoro, N. Yanai, A.-Y. Jee and S. Granick, *Acc. Chem. Res.*, 2014, **47**, 459–469.
5 (*a*) R. J. Kuppler, D. J. Timmons, Q.-R. Fang, J.-R. Li, T. A. Makal, M. D. Young, D. Yuan, D. Zhao, W. Zhuang and H.-C. Zhou, *Coord. Chem. Rev.*, 2009, **253**, 3042–3066; (*b*) S. Bhattacharjee, J. S. Choi, S. T. Yang, S. B. Choi, J. Kim and W. S. Ahn, *J. Nanosci. Nanotechnol.*, 2010, **10**, 135–141; (*c*) S. Ma, J. M. Simmons, D. Sun, D. Yuan and H.-C. Zhou, *Inorg. Chem.*, 2009, **48**, 5263–5268.
6 (*a*) M. Murugesu, R. Clérac, W. Wernsdorfer, C. E. Anson and A. K. Powell, *Angew. Chem., Int. Ed.*, 2005, **44**, 6678–6682, (*Angew. Chem.*, 2005, **117**, 6836–6840); (*b*) T. Liu, Y. J. Zhang, Z. M. Wang and S. Gao, *J. Am. Chem. Soc.*, 2008, **130**, 10500–105001; (*c*) Z. M. Zhang, Y. G. Li, S. Yao, E. B. Wang, Y. H. Wang and R. Clérac, *Angew. Chem., Int. Ed.*, 2009, **48**, 1581–1584, (*Angew. Chem.*, 2009, **121**, 1609–1612).
7 (*a*) P. Horcajada, T. Chalati, C. Serre, B. Gillet, C. Sebrie, T. Baati, J. F. Eubank, D. Heurtaux, P. Clayette, C. Kreuz, J. S. Chang, Y. K. Hwang, V. Marsaud, P. N. Bories, L. Cynober, S. Gil, G. Férey, P. Couvreur and R. Gref, *Nat. Mater.*, 2009, **9**, 172–180; (*b*) S. R. Miller, D. Heurtaux, T. Baati, P. Horcajada, J. M. Greneche and C. Serre, *Chem. Commun.*, 2010, **46**, 4526–4528.
8 (*a*) G. Combarieu, M. Morcrette, F. Millange, N. Guillou, J. Cabana, C. P. Grey, I. Margiolaki, G. Férey and J. M. Tarascon, *Chem. Mater.*, 2009, **21**, 1602–1611; (*b*) G. Férey, F. Millange, M. Morcrette, C. Serre, M. L. Doublet, J. M. Greneche and J. M. Tarascon, *Angew. Chem., Int. Ed.*, 2007, **46**, 3259–3263, (*Angew. Chem.*, 2007, **119**, 3323–3327); (*c*) R. Canioni, C. Roch-Marchal, F. Sécheresse, P. Horcajada, C. Serre, M. Hardi-Dan and Y. K. Hwang, *Mater. Chem.*, 2011, **21**, 1226–1233; (*d*) S. Bauer, C. Serre, T. Devic, P. Horcajada, J. Marrot, G. Férey and N. Stock, *Inorg. Chem.*, 2008, **47**, 7568–7576.
9 M. H. Zeng, X. L. Feng and X. M. Chen, *Dalton Trans.*, 2004, 2217–2223.
10 S. H. Chae, H.-C. Kim, Y. S. Lee, S. Huh, S.-J. Kim, Y. Kim and S. J. Lee, *Cryst. Growth Des.*, 2015, **15**, 268.
11 T. Loiseau, C. Serre, C. Huguenard, G. Fink, F. Taulelle, M. Henry, T. Bataille and G. Férey, *Chem. – Eur. J.*, 2004, **10**, 1373–1382.
12 R.-J. Li, M. Li, X.-P. Zhou, D. Li and M. O'Keeffe, *Chem. Commun.*, 2014, **50**, 4047–4049.
13 K. Sumida, D. L. Rogow, J. A. Mason, T. M. McDonald, E. D. Bloch, Z. R. Herm, T.-H. Bae and J. R. Long, *Chem. Rev.*, 2012, **112**, 724–781.
14 http://www.chem.gla.ac.uk/~louis/software/platon/; A. L. Spek, *Acta Crystallogr., Sect. D: Biol. Crystallogr.*, 2009, **65**, 148–155.
15 I. B. Martini, I. M. Craig, W. C. Molenkamp, H. Miyata, S. H. Tolbert and B. J. Schwartz, *Nat. Nanotechnol.*, 2007, **2**, 647–652.
16 (*a*) A. Poddubny, I. Iorsh, P. Belov and Y. Kivshar, *Nat. Photonics*, 2013, **7**, 948–957; (*b*) N. I. Zheludev and Y. S. Kivshar, *Nat. Mater.*, 2012, **11**, 917–924.
17 (*a*) Y. Tang, W. He, Y. Lu, J. Fielden, X. Xiang and D. Yan, *J. Phys. Chem. C*, 2014, **118**, 25365–25373; (*b*) W. W. Lestari, P. Lönnecke, M. B. Sárosi, H. Cerqueira Streit, M. Adlung, C. Wickleder, M. Handke, W.-D. Einicke, R. Gläser and E. Hey-Hawkins, *CrystEngComm*, 2013, **15**, 3874–3884; (*c*) W. W. Lestari, P. Lönnecke, H. Cerqueira Streit, M. Handke, C. Wickleder and E. Hey-Hawkins, *Eur. J. Inorg. Chem.*, 2014, 1775–1782; (*d*) W. W. Lestari, H. Cerqueira Streit, P. Lönnecke, C. Wickleder and E. Hey-Hawkins, *Dalton Trans.*, 2014, **43**, 8188–8195; (*e*) W. W. Lestari, P. Lönnecke, H. Cerqueira Streit, F. Schleife, C. Wickleder and E. Hey-Hawkins, *Inorg. Chim. Acta*, 2014, **421**, 392–398; (*f*) Z. Hu, B. J. Deibert and J. Li, *Chem. Soc. Rev.*, 2014, **43**, 5815–5840.
18 M. Born and E. Wolf, *Principles of Optics*, 4th edn, 1970, p. 63.
19 G. Ghosh, *Opt. Commun.*, 1999, **163**, 95–102.
20 W. L. F. Armarego and C. L. L. Chai, *Purification of Laboratory Chemicals*, 6th edn, Butterworth-Heinemann (Elsevier), 2009.
21 M. Horie, T. Sassa, D. Hashizume, Y. Suzaki, K. Osakada and T. Wada, *Angew. Chem., Int. Ed.*, 2007, **46**, 4983–4986, (*Angew. Chem.*, 2007, **119**, 5071–5074).
22 S.-H. Yang, M. L. Cooper, P. R. Bandaru and S. Mookherjea, *Opt. Express*, 2008, **16**, 8306–8316.
23 K. Okano, O. Tsutsumi, A. Shishido and T. Ikeda, *J. Am. Chem. Soc.*, 2006, **128**, 15368–15369.
24 (*a*) Z. Wang and S. Hi, *J. Serb. Chem. Soc.*, 2008, **73**, 1187–1196; (*b*) http://www.photonics.com/Category.aspx?CatID=19950.
25 P. G. Del Rosso, M. F. Almassio, M. Bruno and R. O. Garay, *Tetrahedron Lett.*, 2010, **51**, 6730–6733.
26 N. Miyaura, K. Yamada and A. Suzuki, *Tetrahedron Lett.*, 1979, **20**, 3437–3440.
27 *CrysAlis Pro*, Oxford Diffraction Ltd, Oxfordshire, U.K., 2010.
28 *SCALE3 ABSPACK*, Oxford Diffraction Ltd., Oxfordshire, U.K., 2010.
29 SHELXL: G. M. Sheldrick, *Acta Crystallogr., Sect. C: Cryst. Struct. Commun.*, 2015, **71**, 3–8.